iScience

CellPress
OPEN ACCESS

Article

# Ripening of two-dimensional colloidal CdSe nanocrystals into zero-dimensional nanodots

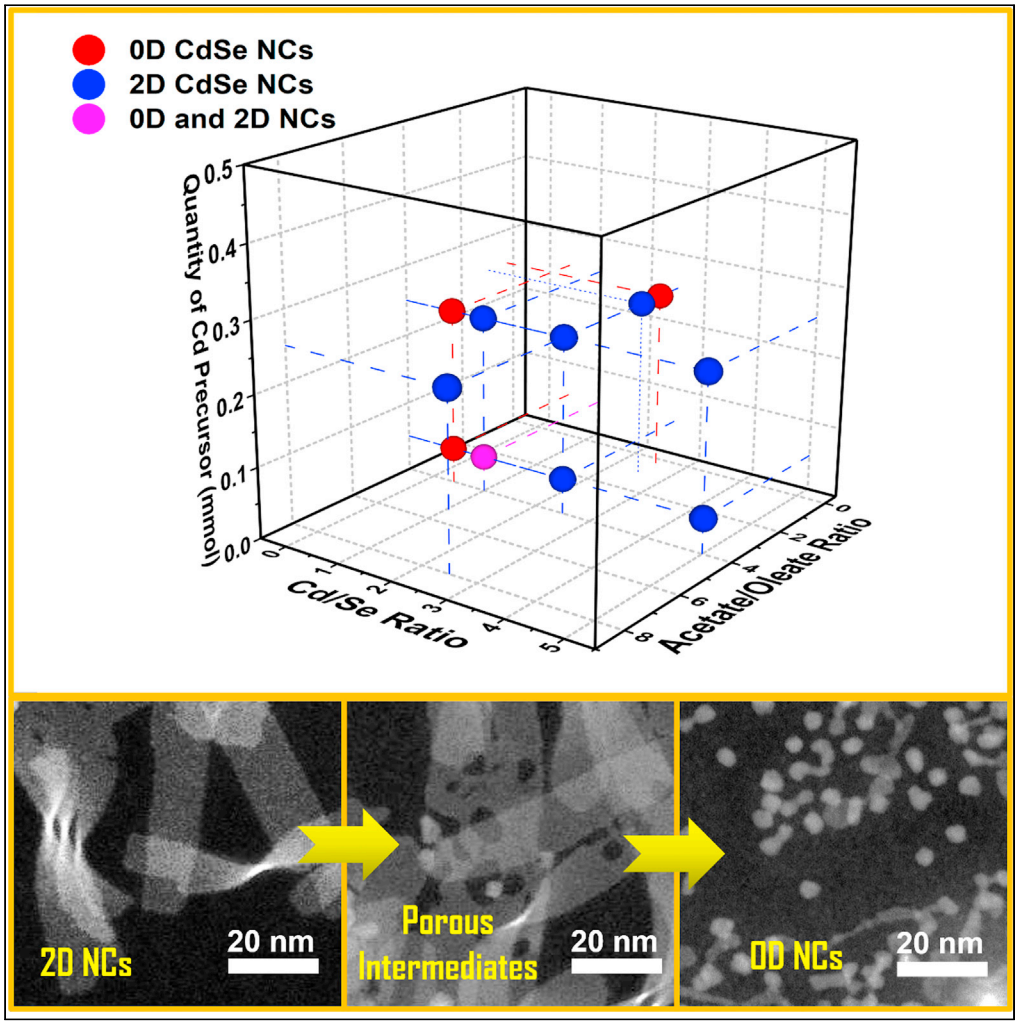


Xiaopeng Huang, Virendra K. Parashar, Martin A.M. Gijs

martin.gijs@epfl.ch

## Highlights

The intraparticle ripening of 2D CdSe nanocrystals leads to 0D nanodots

The conditions affecting the ripening of 2D CdSe nanocrystals were studied

Two different intermediates were found during the ripening of 2D CdSe nanocrystals

Huang et al., iScience *24*, 103457
December 17, 2021 
https://doi.org/10.1016/j.isci.2021.103457

iScience

CellPress
OPEN ACCESS

Article

# Ripening of two-dimensional colloidal CdSe nanocrystals into zero-dimensional nanodots

Xiaopeng Huang,[1,2] Virendra K. Parashar,[1] and Martin A.M. Gijs[1,3,*]

## SUMMARY

**Understanding the ripening of two-dimensional (2D) colloidal nanocrystals (NCs) is important for the controllable synthesis of NCs with desired morphology and properties. In this study, we systematically investigate the ripening behavior of the 2D CdSe NCs in the presence of a short-chain acetate ligand and a long-chain oleate ligand. We find that a low acetate/oleate ratio, a low Cd/Se ratio, and a low monomer concentration help in the ripening of the 2D NCs to form 0D NCs. Moreover, a porous nanosheet intermediate is observed when there is a high Cd/Se ratio, whereas in the case of a low Cd/Se ratio, the ripening starts from the edge of the nanosheets, resulting in a saw-like nanosheet intermediate. These findings provide necessary insights into the growth and ripening of 2D CdSe NCs that allow for the controlled synthesis of 0D and 2D CdSe NCs.**

## INTRODUCTION

Two-dimensional (2D) colloidal CdSe nanocrystals (NCs) form a new class of semiconductor nanomaterials with atomically flat surfaces and exhibit a large number of shapes, such as nanoplatelets, nanoribbons, nanodisks, nanobelts, and nanoscrolls. They have intrigued tremendous attention owing to their exceptional optoelectronic properties, such as a pure photoluminescence peak, a high absorption cross-section, a large exciton binding energy, and a large optical gain (Berends and de Mello Donega, 2017; Bouet et al., 2013; Son et al., 2011; Wang et al., 2015; Yu and Chen, 2020). Owing to the numerous efforts from the academic community, great progress has been achieved in the past decade, showing the successful synthesis of 2D CdSe NCs with highly adjustable thickness and lateral dimension, as well as some heterogeneous architectures such as core-shell and core-crown nanostructures (Bertrand et al., 2016; Cho et al., 2018; Mahler et al., 2012; Rossinelli et al., 2017). These works have laid a solid foundation for the application of the new nanostructures in a wide range of fields, such as optoelectronics, lasing, and bioimaging (Chen et al., 2014; She et al., 2014, 2015).

It has been widely acknowledged that flat 2D CdSe nanostructures obtained from a colloidal solution are kinetically stable products, which would undergo a series of shape changes as the reaction evolves (Cunningham et al., 2020; Riedinger et al., 2017). Many studies have investigated the shape evolution of the 2D NCs, with particular focus on the crystal growth stage to obtain NCs with desired morphologies and properties (Ithurria et al., 2011a; Li and Peng, 2011). However, little attention was paid to the shape evolution in the ripening stage, in which the kinetically stable 2D configuration would turn into a more thermodynamically stable morphology as a result of reduced monomer sources (Christodoulou et al., 2018; Lee et al., 2003). In our previous work, we demonstrated that there was no clear boundary in the growth conditions for forming either 2D CdSe NCs or 0D NCs (Huang et al., 2019, 2020). The former are kinetically stable, while the latter are thermodynamically stable; the conversion between the two configurations can be achieved by adjusting the length of the carboxylate ligand used in the colloidal solution, the monomer concentration, as well as the reaction temperature. We also had a preliminary finding that the initially formed well-defined 2D CdSe NCs would gradually turn into 0D CdSe NCs after a prolonged reaction time, which is known as intraparticle ripening behavior (Huang et al., 2020). The longer the carboxylate ligand is, the earlier the intraparticle ripening takes place. It is clear that the ripening behavior of the NCs has a close relationship with their anisotropic growth, which might reveal the formation mechanism of NCs from another perspective (Peng and Peng, 2001). The thermal stability of anisotropic NCs obtained for a given synthetic condition is also highly influenced by the nature of the ripening stage (Li and Peng, 2011). Moreover, adjusting the ripening behavior of the 2D CdSe NCs can open up an avenue to enhance the control over the shape, structure, and property of the NCs. Therefore, a further study on the ripening behavior of the 2D CdSe NCs is of great importance for the controlled synthesis and applications of the nanostructures.

[1]Laboratory of Microsystems, Ecole Polytechnique Fédérale de Lausanne (EPFL), 1015 Lausanne, Switzerland

[2]Chemistry Research Laboratory, Department of Chemistry, University of Oxford, 12, Mansfield Road, Oxford OX1 2JD, UK

[3]Lead contact

*Correspondence: martin.gijs@epfl.ch

https://doi.org/10.1016/j.isci.2021.103457

In this work, we investigate the intraparticle ripening behavior of the 2D CdSe NCs, and explore the favorable and unfavorable conditions for the transformation of 2D NCs to their 0D ripened products. The detailed ripening process as well as their possible ripening mechanism will also be discussed. Transmission electron microscopy (TEM), high-resolution TEM (HRTEM), high-angle annular dark-field scanning transmission electron microscopy (HAADF-STEM), ultraviolet-visible (UV–vis) absorption, photoluminescence (PL) spectroscopies, and powder X-ray diffraction (XRD) spectra were used to characterize the shape evolution of the CdSe NCs in a given reaction condition. Fourier transform infrared spectroscopy (FTIR) and thermal gravimetric analysis (TGA) were used to analyze the capping ligands on the surface of the NCs.

## RESULTS AND DISCUSSION

### Ripening of colloidal CdSe nanotubes and nanosheets

We previously reported the formation of CdSe nanotubes via the angular and lateral attachment of 2D nanoplatelet building blocks in the presence of acetate and dioctylamine ligands (Huang et al., 2019). Based on similar synthetic protocols, here, we investigated the influence of concurrent use of acetate and a medium-/long-chain carboxylate on the shape evolution of the 2D CdSe NCs. By reacting a cadmium acetate in dioctylamine ($Cd(acetate)_2$-DOAm) solution with a trioctyl phosphine selenide (TOP-Se) solution for 8 min, we obtained multiwalled CdSe nanotubes of 20–50 nm in diameter and 100–200 nm in length (Figures 1A and S1F), which were nanostructures evolved from curved multilayered nanosheets (Figure S1A). These nanotubes are easily aggregated owing to the absence of long-chain carboxylate ligands. The absorption spectra of the nanotubes show characteristic peaks at 444 nm and 474 nm, which can be attributed to light-hole and heavy-hole transition, indicating that the nanotubes have atomically flat walls of 3.5 molecular monolayers (MLs) in thickness (Figures 1C and S1K) (Ithurria et al., 2011b). Extended the reaction time up to 256 min, and the tubular nanostructures were seen to be decomposed, ripening into highly aggregated spherical nanodots with the size of several nanometers (Figures 1B and S2). The absorption spectra show no clear characteristic excitonic peak, demonstrating that these particles are too big and thus no quantum confinement effect is observed (Figure 1C).

When hexanoate was synchronously added during the reaction, monodisperse tube-like nanostructures of 20–40 nm in diameter and 200–400 nm in length were observed within a reaction time of 1 min (Figures 1D and S1B). The ripening of these nanotubes occurred within a reaction time of 8 min, turning into broken nanosheets and dot-like nanostructures (Figures 1E and S1G). Similar results were also found in the case of synchronously adding octanoate, in which the tubular nanostructures show a higher degree of disintegration into sheet-like and dot-like nanostructures within a reaction time of 8 min (Figures S1C and S1H). In the case of using laureate, we could still see some tubular nanostructures, but more and more sheet-like nanostructures appeared within a reaction time of 1 min (Figure S1D). Moreover, the tubular nanostructures decomposed more strongly into dot-like nano-objects within a reaction time of 8 min (Figure S1I). The absorption spectra of these three samples look similar, showing a shift of the main characteristic peaks from 376 nm and 397 nm to 437 nm and 464 nm, corresponding to the thickness growth of 2D CdSe NCs from 2.5 MLs to 3.5 MLs (Ithurria et al., 2011b) (Figures 1F and S1L–S1N). When oleate was used, no tubular structure but only nanosheets of 40–70 nm in length and 10–30 nm in width were found within a reaction time of 1 min (Figures 1G and S1E). Ripening of these nanosheets results in the formation of nanodots of 4–8 nm in size within a reaction time of 64 min (Figure 1H). A characteristic excitonic peak at 581 nm was found, which is an indication of the presence of 0D CdSe nanodots with a quantum confinement effect (Figure 1I). These results suggest that with additional medium-/long-chain carboxylates added to the protocol of CdSe nanotubes synthesis, the tubular nanostructures would evolve into sheet-like nanostructures; the longer the additional carboxylate ligand is, the more abundant the nanosheets would be. Moreover, as the reaction evolved, the initially formed nanotubes and nanosheets ripened into more thermodynamically stable dot-like nanostructures (Figure 1J). These results are consistent with our previous insight that the formation of the CdSe nanotubes is due to the low orientational degree of freedom of the nanoplatelet building blocks inside the solid Cd precursor matrix. Adding medium-/long-chain carboxylates would 1) facilitate the mobility of the nanoplate building blocks in the organic solvent, resulting in more nanosheets with better dispersibility, and 2) promote the intraparticle ripening of the nanotubes and nanosheets into more monodispersed nanodots. These observations and hypotheses motivated us to perform a systematic study of the ripening behavior of CdSe NCs.

We first focused our study on the ripening process of the 2D CdSe nanosheets prepared by using simultaneously acetate and oleate at a molar ratio of 1:1 between acetate and oleate. As shown in Figures 2A and

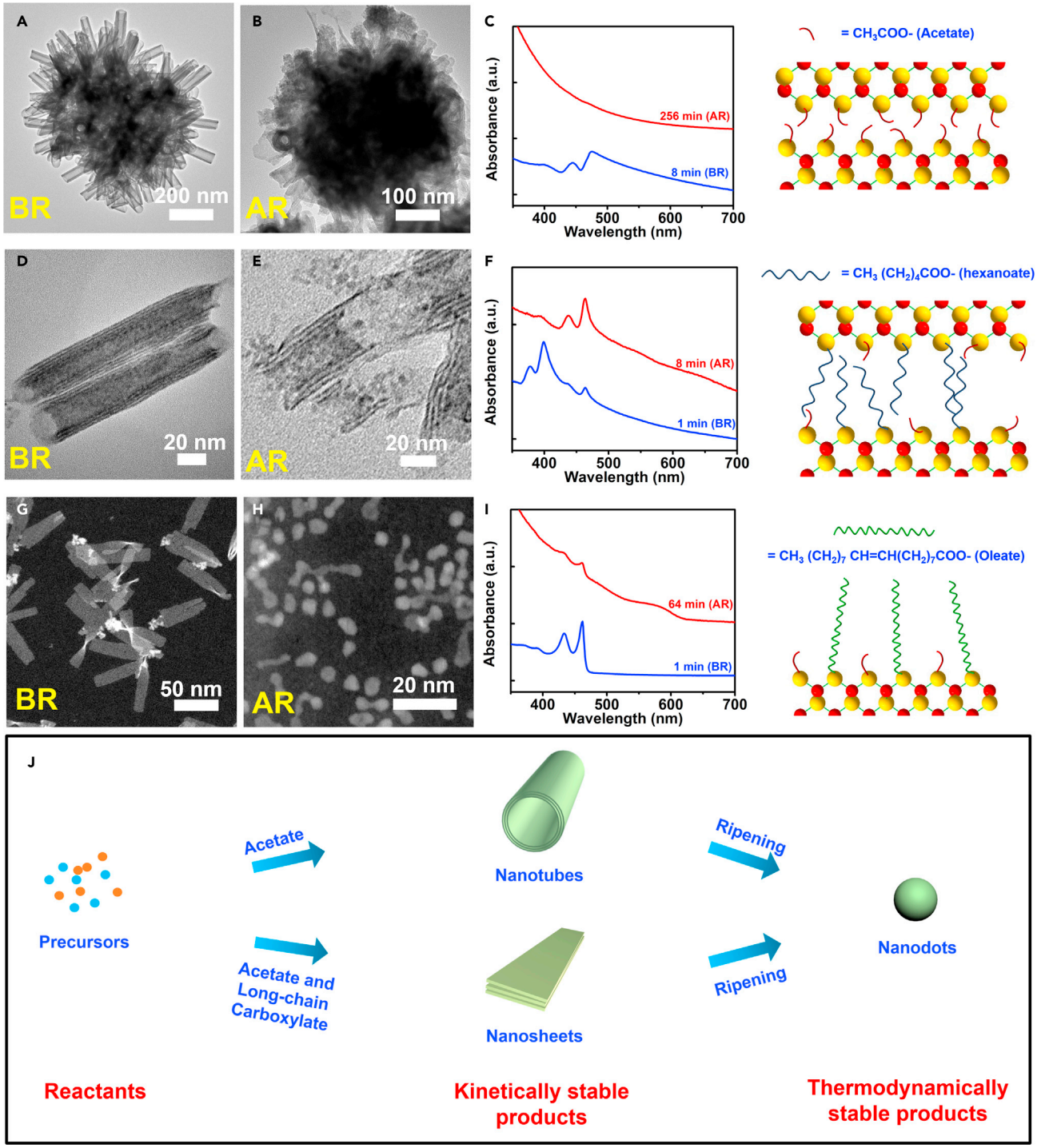


**Figure 1. Ripening of the CdSe NCs synthesized in the presence of different comibinations of carboxylate ligands**

(A–I) (A, B, D, and E) TEM images, (G and H) STEM images, and (C, F, and I) UV-vis absorption spectra of CdSe NCs synthesized in the presence of only acetate (A–C), acetate and hexanoate (D–F), and acetate and oleate (G–I) within a reaction time of 1 min (BR; D and G), 8 min (BR or AR; A and E), 64 min (AR; H), and 256 min (AR; B), respectively. The right panel shows the schematic illustrations of the possible surface ligand capping for NCs before ripening in each case. (J) A schematic showing that the kinetically stable CdSe nanotubes and nanosheets, formed under different combinations of carboxylate ligands respectively, turn into thermodynamically stable nanodots after ripening.

BR, before ripening; AR, after ripening.

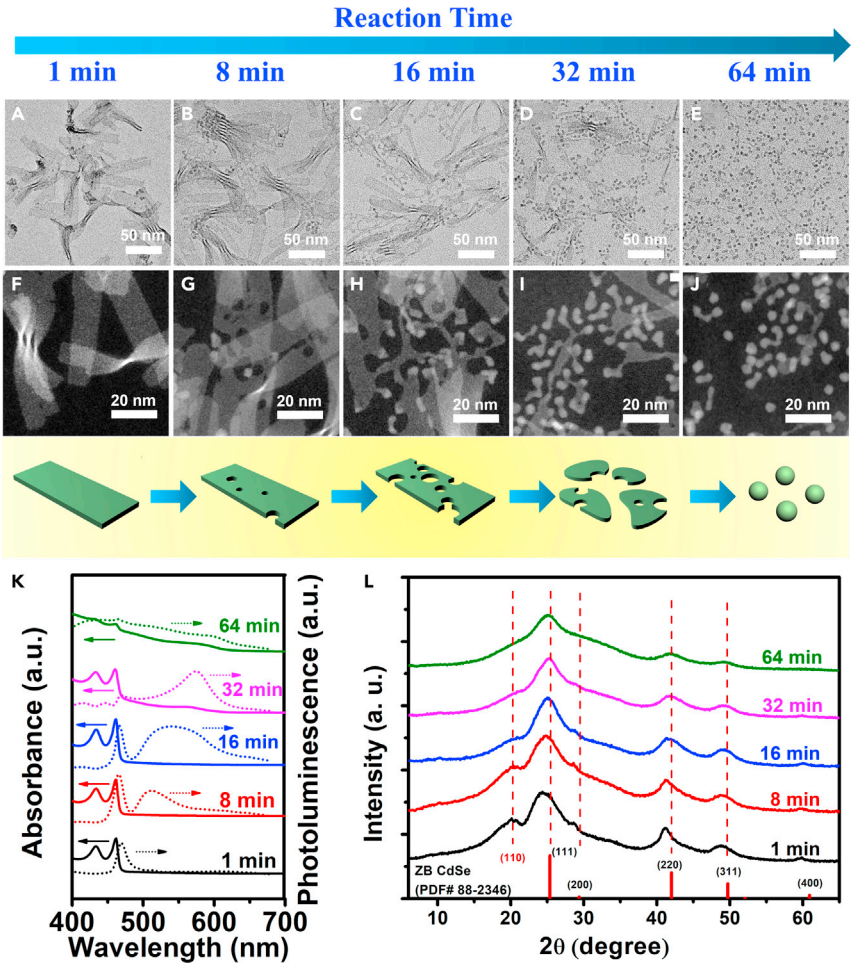


**Figure 2. Ripening process of the 2D CdSe nanosheets synthesized in the presence of acetate and oleate**

(A–L) (A–E) TEM images, (F–J) STEM images, (K) absorption spectra, and (L) powder XRD spectra of the CdSe NCs synthesized in the presence of acetate and oleate within a reaction time of 1 min (A and F), 8 min (B and G), 16 min (C and H), 32 min (D and I), and 64 min (E and J), respectively. The schematic in the yellow panel corresponds to the morphologies of the NCs in the same column.

2F, well-defined CdSe nanosheets obtained within a reaction time of 1 min show a characteristic main absorption peak at 462 nm and a sharp photoluminescence peak at 470 nm with a full width at half maximum (fwhm) of 14 nm, which is similar to the classical 2D zincblende CdSe NCs reported by other groups (Ithurria and Dubertret, 2008). Within a reaction time of 8 min, holes of 1–10 nm in diameter appeared in the middle of the nanosheets, accompanied by the presence of platelet-like fragments with diameters of 2–5 nm (Figures 2B and 2G). The broad photoluminescence peaks at 512 nm with an fwhm of 53 nm can be attributed to the deep trap emission of the small CdSe nanoplatelets (Figure 2K) (Ithurria et al., 2011a). The nanosheets continued to disintegrate into small-size nanoplatelet fragments within a reaction time of 16 min, which shows a very broad photoluminescence peak at 542 nm with an fwhm of 110 nm (Figures 2C and 2H). As the reaction continued for 32 min, the absorption peak at 462 nm corresponding to 2D CdSe NCs was broadened, and a broad peak at 562 nm corresponding to 0D CdSe NCs appeared, along with a strong yet broad photoluminescence peak at 575 nm with an fwhm of 54 nm. This suggests that the nanoplatelet fragments have gradually turned into nanodots with a diameter of 3–4 nm via intraparticle ripening, as evidenced by the appearance of some dot-like CdSe NCs shown in Figures 2D and 2I. Further increasing the reaction time to 64 min results in more 0D nanodots and less 2D nanosheets, which is consistent with the weakening of the absorption peak at 462 nm corresponding to 2D CdSe NCs. The broad photoluminescence spectrum spanning between 400 nm and 700 nm is attributed to a combination of the decomposed nanosheets, nanoplatelet fragments, and ripened nanodots. Powder XRD spectra in Figure 2L further

confirm the transformation of 2D nanosheets to 0D CdSe nanodots. Within a reaction of 1 min, characteristic peaks of 2D CdSe NCs are found, including the appearance of (110) peak, the enhancement of (200), (220), and (400) peaks, as well as the shift of main peaks in the low-angle direction (Huang et al., 2020). These features gradually disappear with reaction time. Within a reaction of 64 min, the XRD pattern only shows the peaks of nanodots, which is basically similar to the bulk zincblende CdSe crystals. The peaks of 0D nanodots are broader than those of 2D nanosheets, suggesting that the crystal grains in the nanodots are smaller. As depicted in the yellow panel of Figure 2, the above phenomena clearly demonstrate that the ripening of CdSe nanosheets would start by producing some nanoscale holes on the interior of nanosheets and forming nanoplatelet fragments, followed by a transformation into nanodots. It should be noted that this ripening behavior does not only occur in the 2D NCs prepared in the concurrent use of a short-chain and a medium-/long-chain ligand. In CdSe nanosheets synthesized solely by using a butyrate ligand, similar intermediates showing porous nanosheets intermediates and nanoplatelet fragments were also found within a reaction time of 128 min (Figure S3).

## Favorable conditions for the ripening of 2D CdSe NCs

Furthermore, we studied the favorable conditions for the intraparticle ripening of 2D CdSe NCs into 0D nanodots. The influence of the molecular ratio between the shorter acetate ligand and the longer oleate ligand was first investigated by gradually increasing the content of oleic acid, which coordinates to the Cd center in the form of oleate. As shown in Figure S4, with increasing oleate quantity from 0.0625 mmol to 0.125 mmol, 0.5 mmol and 2 mmol, the shape of the CdSe NCs changes from highly agglomerated multilayered nanosheets (Figure S4A) to more dispersed nanosheets with shorter lateral dimension (Figures S4B–S4D) and finally to branched nanorods (Figure S4E) within a reaction time of 1 min. This is in accordance with our previous findings that short-chain carboxylate ligands are beneficial for the 2D growth of NCs in the reaction-limited growth mode, while long-chain ligands favor the growth of NCs in the diffusion-limited mode and produce 0D/1D nanostructures (Huang et al., 2020). When acetate is the dominant carboxylate ligand, more building blocks for the 2D NCs would be produced and assembled into 2D nanostructures with a larger lateral dimension. When more oleate is added, 2D growth of the NCs is inhibited, yet their dispersibility becomes better as a result of the long-chain ligand passivation. Eventually, as oleate dominates the surface capping of the NCs, more thermodynamically stable building blocks would generate and assemble to form 1D branched nanorods. The absorption spectra indicate that the nanosheets have a thickness characterized by either a mixture of 2.5 MLs and 3.5 MLs (Figures S4L andS4M) or solely of 3.5 MLs (Figure S4N). Extending the reaction time to 8 min, the NCs grow into nanotubes in the absence of oleate and large-size nanosheets at an oleate quantity of 0.0625 mmol, respectively (Figures S4F andS4G). At molar ratios of 1:0.25 and 1:1 between acetate and oleate, we observed porous nanosheet intermediates (Figures S4H andS4I), which is an indication of ripening. The absorption spectra demonstrate that the nanosheets have a thickness of 3.5 MLs at this stage (Figures S4L–S4N). The branched nanorods formed in the presence of 2.0 mmol oleate turned into more isotropic nanodots by intraparticle ripening at a reaction of 8 min, similar to the case of solely using oleate ligand, as previously reported (Figure S4J) (Huang et al., 2020). Their absorption spectra show characteristic broad peaks of 0D/1D CdSe NCs, with the absorption maximum shifts from around 560 nm–600 nm, corresponding to a size change of the nanodots from 3.3 nm to 4.6 nm (Figure S4O) (Huang et al., 2018; Peng et al., 2000; Yu et al., 2003). In short, adding the long-chain carboxylate ligand will restrain the 2D growth of CdSe NCs and accelerate their intraparticle ripening to form 0D NCs.

Then, we studied the influence of the molar ratio between the cationic and anionic precursors on the ripening of the NCs. As shown in Figure 3, we fixed the quantity of Cd precursor at 0.25 mmol and gradually increased the amount of Se precursor from 0.05 mmol to 0.625 mmol. Within a reaction time of 1 min, we obtained ultrathin CdSe nanosheets in all the cases. As more Se precursor was added, the lateral dimensions of the nanosheets became smaller, changing from 60–80 nm in length at a Cd/Se ratio of 0.25:0.05 to 10–30 nm in length at a Cd/Se ratio of 0.25:0.625 (Figures 3A–3D). Some CdSe nanoparticle aggregates larger than 10 nm were visible at a very high Se quantity of 0.625 mmol (Figure 3D). The absorption spectra reveal that most of the nanosheets at this stage are characterized by two populations of thicknesses, namely 2.5 MLs and 3.5 MLs (Figures 3I–3L). Within a reaction time of 8 min, the nanosheets synthesized with 0.05 mmol and 0.1 mmol Se precursor continued to grow laterally, suggesting that a high Cd/Se ratio benefited the continuous growth of NCs into larger size nanosheets. Conversely, in the case of using 0.25 mmol Se precursor, the nanosheets started to ripen, turning into some saw-like nanosheets (Figure 3G). Interestingly, this nanostructure is very different from the aforementioned porous nanosheet

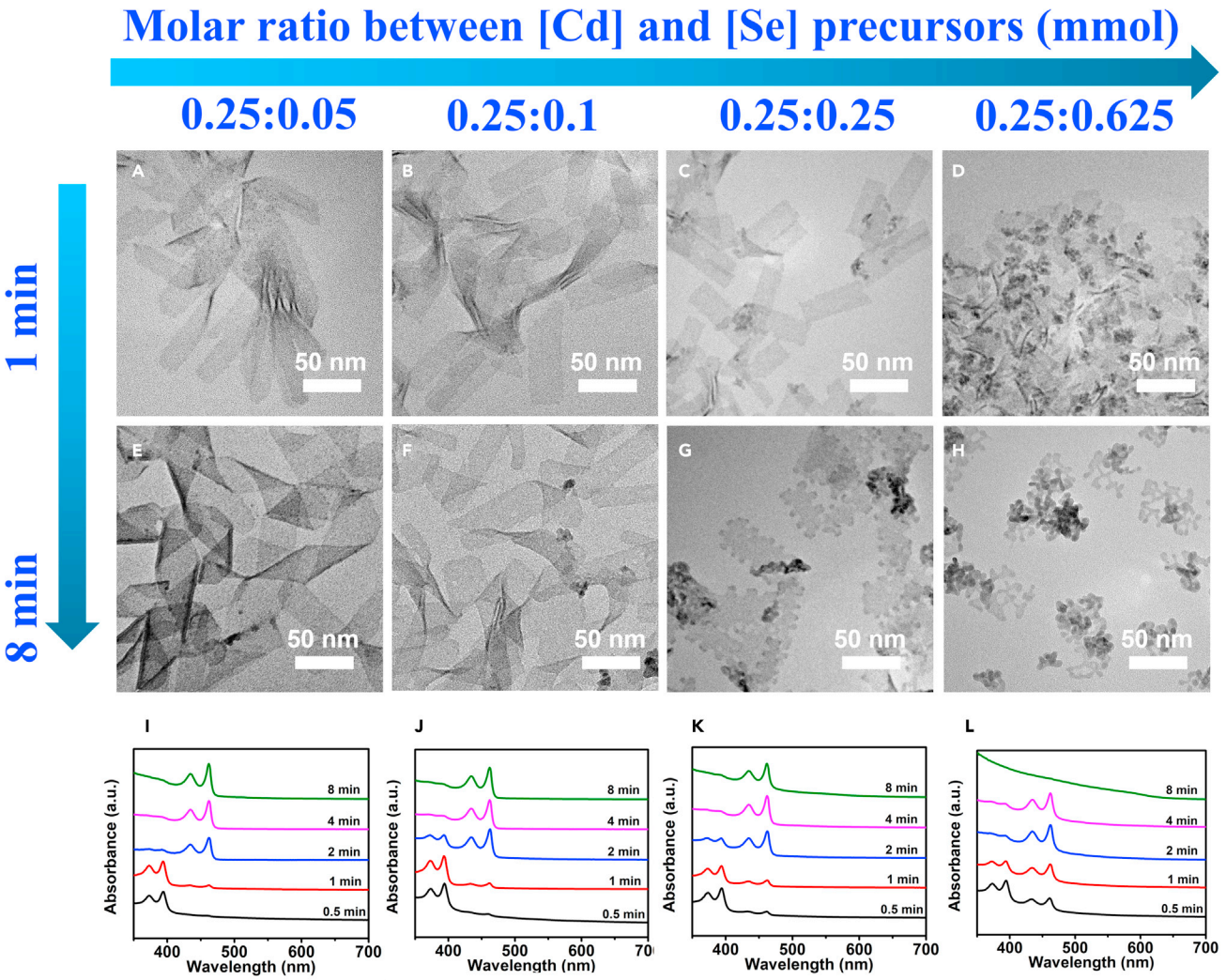


**Figure 3. Ripening of the 2D CdSe nanosheets at a high monomer concentration and different Cd/Se ratios**

(A–L) (A–H) TEM images and (I–L) absorption spectra of the CdSe NCs synthesized in the presence of acetate and oleate at the quantity of 0.25 mmol and 0.05 mmol (A and E), 0.25 mmol and 0.1 mmol (B and F), 0.25 mmol and 0.25 mmol (C and G), and 0.25 mmol and 0.625 mmol (D and H) between Cd and Se precursors, respectively, within a reaction time of 1 min (A–D) and 8 min (E–H). The molar ratios between acetate and oleate are kept at 1: 0.25 in all cases.

intermediates, which will be further discussed below. In the case of using 0.625 mmol Se precursor, the ripened CdSe nanostructures were like the evolved products of the saw-like intermediates, showing highly aggregated branch-like and dot-like nanoparticles (Figure 3H). No peak of 2D NCs was found in their absorption spectra, which shows a broad scattering peak and a tiny excitonic peak at 600 nm (Figure 3L). All these investigations suggest that a high Cd/Se ratio would favor the formation of 2D CdSe nanosheets, while a low Cd/Se ratio helps in the production of isotropic 0D nanodots aggregates, particularly after intraparticle ripening.

Next, we investigated the influence of the monomer concentration on the ripening of NCs by varying the concentration of the precursor solutions. Keeping all the other conditions constant, we reduced the quantity of the Cd and Se precursors to one-fifth of the samples shown in Figure 3. At the early stage of the reaction, we obtained ultrathin CdSe nanosheets of 3.5 MLs in thickness when the added Cd/Se ratios were 0.05:0.01, 0.05:0.02, and 0.05:0.01 (Figures S5A–S5C and S5I–S5K). At the Se content of 0.125 mmol, even though there is still a weak absorption peak at 462 nm corresponding to 3.5-ML nanosheets, the vast majority of the products are ascribed to 0D/1D NCs with a characteristic peak at 550 nm

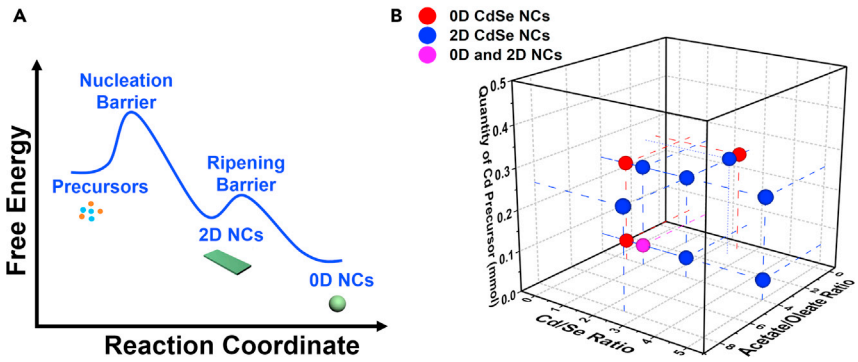


**Figure 4. Favorable conditions for the ripening of 2D CdSe nanosheets into 0D nanodots**

(A) A schematic showing the growth of 2D NCs and their ripening into 0D NCs in terms of Gibbs free energy.

(B) A plot showing the obtained main CdSe NCs synthesized within a reaction time of 8 min at different acetate/oleate ratios, Cd/Se ratios, and precursor contents.

(Figure S5L). This is in good agreement with the TEM and STEM images exhibiting a mixture of chain-like nanorods and spherical nanodots (Figure S5D). Increasing the reaction time to 8 min, similar to the trend observed at the high precursor concentration in Figure 3, nanosheets synthesized with the low Se content of 0.01 mmol and 0.02 mmol continued to grow laterally, some of which even curled into scroll-like nanostructures (Figures S5E andS5F). At higher Se content of 0.05 mmol, the nanosheets were ripened into broken nanosheets and spherical nanodots with an excitonic absorption peak at 540 nm (Figures S5G andS5K). The chain-like NCs formed at the Se content of 0.125 mmol were also ripened into more monodisperse nanodots with high crystallinity (Figure S5H). Compared with the cases of a high monomer concentration displayed in Figure 3, a low monomer concentration shows a clear trend of accelerating the intraparticle ripening of the NCs.

## Possible mechanism for the ripening of 2D CdSe NCs

In an effort to understand our experimental observations, according to the LaMer model, a classical crystal growth route would encompass several stages including monomer accumulation, nucleation, growth, and ripening (LaMer and Dinegar, 1950; Whitehead et al., 2019), depending on the change of monomer concentration during the reaction. As the reaction evolves, the free monomers are gradually consumed down to a low level, finally being unable to support the growth of further NCs. The NCs will however continue to grow by ripening, either by interparticle ripening (e.g. Ostwald ripening) or intraparticle ripening. With respect to anisotropic NCs having kinetically stable shapes (e.g. 2D CdSe NCs), high-energy facets would dissolve back to monomers, diffusing and depositing on the less active facets, eventually forming a more thermodynamically stable morphology (e.g. 0D CdSe NCs), which is known as intraparticle ripening (You and Fang, 2016). As shown in Figure 4A, there exists a ripening energy barrier where the growth via monomer feeding and via decomposition of early formed particles reaches an equilibrium. This barrier is closely related to the local growth environment of the NCs. Based on the above investigations, Figure 4B discloses that a low acetate/oleate ratio, a low Cd/Se ratio, and a low monomer concentration are helpful to reduce the ripening barrier, therefore accelerating the transformation of 2D CdSe nanosheets to 0D nanodots via intraparticle ripening. The influence of a low acetate/oleate ratio and a low monomer concentration can be easily understood, as these conditions lead to a diffusion-controlled growth, which is in favor of the formation of thermodynamically stable 0D nanodots (Huang et al., 2020). Besides, as ultrathin 2D CdSe NCs require an additional Cd layer in the (001) basal plane, a high Cd/Se ratio is responsible for the stability of the 2D configuration (Li and Peng, 2011). We also found that two kinds of intermediates present during the ripening of the 2D NCs: porous nanosheet intermediates in the case of a high Cd/Se ratio and saw-like nanosheet intermediates when the Se ratio is increased. Compared with the intraparticle ripening of other anisotropic NCs such as CdSe nanorods and Au nanoparticles (Peng and Peng, 2001; Uematsu et al., 2014), this is an interesting and novel growth behavior, which deserves further study.

The starting points of intraparticle ripening are typically some high-energy sites, such as surfaces, edges, vertexes as well as defects, which are greatly dependent on the crystal growth mechanism. In the NCs formed via a classical monomer addition approach, the stepwise deposition of the molecule-level

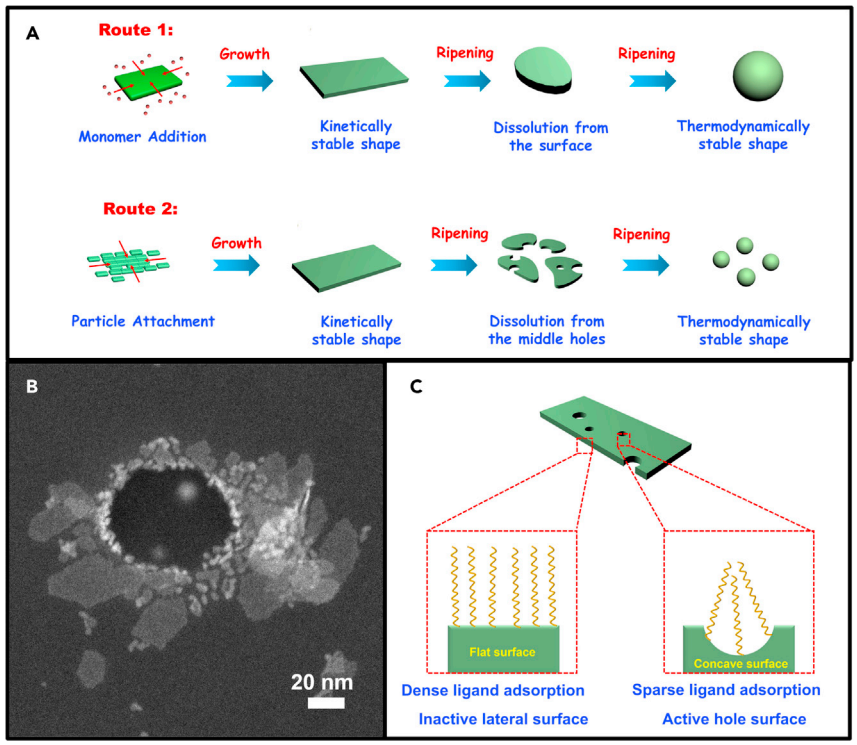


**Figure 5. A possible mechanism for the formation of porous nanosheet intermediates**

(A) A schematic showing the ripening processes involved in two different crystal growth mechanisms. In route one, where the anisotropic particle is formed by classical monomer addition, the intraparticle ripening is supposed to start from the edge of active facets. Whereas in route two, where the anisotropic particle is formed via non-classical particle attachment, the defects present in the interior of the nanocrystals could be the ripening starting points.

(B) An assembly of nanoplatelets into a tube-like nanostructure observed when the CdSe NCs are synthesized using a quantity of 0.05 mmol and 0.01 mmol for the Cd and Se precursors, respectively, and for a reaction time of 1 min.

(C) A schematic showing the possible arrangement of long-chain ligands on the lateral surface and hole surface of the NCs.

monomers on the initially formed nuclei ensures that there are little defects in the interior of the NCs. In this case, ripening of the NCs would be carried out by dissolving the active surfaces having a large number of dangling bonds, and facilitating the growth of the less active surface (route 1 of Figure 5A), as reported in the 1D/2D ripening of CdSe nanorods (Peng and Peng, 2001). On the other hand, NCs are also frequently found to grow via a non-classical particle attachment route, in which the early formed primary NCs act as building blocks to construct larger anisotropic nanoarchitectures by a series of processes including aggregate, alignment, fusion, and post-recrystallization. Colloidal 2D NCs formed via this route feature the irregular edges and porous patch-like configuration, as observed in the ultrathin PbS nanosheets (Ivanov et al., 2014; Schliehe et al., 2010). A similar phenomenon is also found in the 2D CdSe NCs synthesized in this work, as clearly shown in the early-formed porous CdSe nanosheets in Figure S5A. Moreover, we also observed a clear assembly of nanoplatelets into tube-like nanostructure in the same sample (Figure 5B), which agrees well with our previous finding that the formation of nanotubes is via attachment of nanoplatelet building blocks (Huang et al., 2019). In this regard, the growth of the nanosheets via a particle-mediated approach can well explain the emergence of porous nanosheets intermediates. Furthermore, the surface stability of the CdSe NCs is greatly influenced by the passivation of various long-chain ligands, including carboxylates, amines, and phosphines. As depicted in Figure 5C, the surface of the middle hole with a concave geometry is supposed to be less passivated with ligands compared with the lateral surface owing to the steric hindrance effect of the alkyl chains. As a result, the middle hole is more active and becomes the disintegration center during the intraparticle ripening (route 2 of Figure 5A).

Similarly, the formation of saw-like nanosheet intermediates as displayed in Figure 3G in the presence of a low Cd/Se ratio can also be explained by the surface ligand passivation. When there is a shortage of the Cd

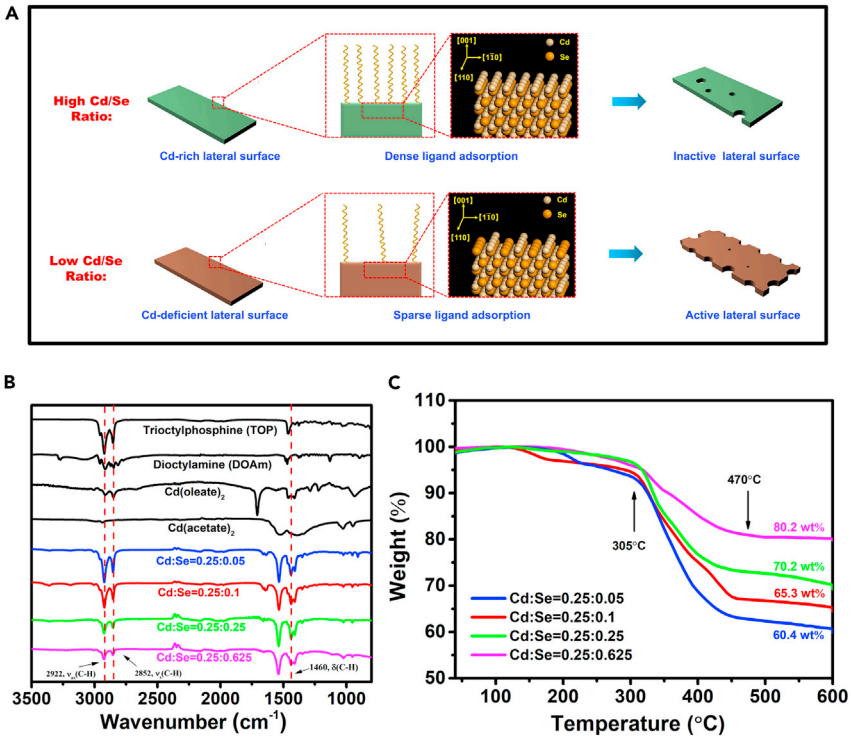


**Figure 6. A possible mechanism for the formation of saw-like nanosheet intermediates**

(A) A schematic showing the possible arrangement of long-chain ligands adsorbed on the lateral surface of the NCs synthesized at high and low Cd/Se ratio, respectively.

(B) FTIR spectra of the surface ligands including TOP, DOAm, $Cd(oleate)_2$, and $Cd(acetate)_2$, as well as the CdSe NCs prepared in the presence of acetate and oleate at the quantity of 0.25 mmol and 0.05 mmol, 0.25 mmol and 0.1 mmol, 0.25 mmol and 0.25 mmol, and 0.25 mmol and 0.625 mmol between Cd and Se precursors, respectively, within a reaction time of 8 min.

(C) TGA weight loss of the CdSe NCs prepared at different quantities of Cd and Se precursors within a reaction time of 8 min. The surface ligands started to combust at 305°C and be totally removed at around 600°C.

precursor, the surface structure of the NCs would reconstruct to have more Se atoms on the surface, such as by stripping off part of surface Cd atoms on the (001) facets (Figure 6A). Different from the surface Cd atoms being passivated with X-type ligands (carboxylates) and L-type ligands (alkylamines and alkylphosphines), the surface Se atoms are capped by Z-type ligands (e.g. cadmium carboxylates in this study), which are also deficient when the quantity of Cd source is low (Anderson et al., 2013; Owen, 2015). Surface Se atoms can also be passivated with alkylphosphines by forming TOPSe, yet the passivation ability is quite low and easy to be removed (Kim et al., 2010; Vondrásek et al., 2009). Consequently, the NCs synthesized with a low Cd/Se ratio would be less passivated. This is supported by the FTIR spectra showing a decreasing characteristic peak of hydrocarbon chains: the characteristic vibration peaks corresponding to the hydrocarbon tails at 2922 $cm^{-1}$, 2852 $cm^{-1}$, and 1460 $cm^{-1}$ gradually decrease as the Se quantity is increased, suggesting that there is a reduced capping of long-chain ligands (Figure 6B). Moreover, the weight loss of the samples in TGA analysis gradually increased as the Se quantity is decreased, which further demonstrates that the CdSe NCs with a low Cd/Se ratio have lower surface passivation by organic ligands (Figure 6C). As a result, the lateral surfaces of the NCs prepared with a low Cd/Se ratio become more active compared with those prepared with a high Cd/Se ratio, therefore allowing that the intraparticle ripening starts from the lateral surface sites and explaining the evenly distributed sawteeth of the ripening intermediates, as the unpassivated Se-terminated sites are homogenously distributed.

## Conclusions

In summary, we have systematically investigated the intraparticle ripening of 2D CdSe NCs under different conditions. The CdSe nanotubes formed in the presence of acetate would evolve into flat sheet-like nanostructures in the case of concurrent use of acetate and medium-/long-chain carboxylates, and completely

become nanosheets when oleate was used. As the reaction proceeds, the 2D nanosheets would transform into 0D nanodots through intraparticle ripening. In most situations where the Cd/Se ratio was high, the intraparticle ripening started by forming some porous nanosheet intermediates, which were disintegrated into nanoplatelet fragments before eventually turning into 0D nanodots. In the case of a low Cd/Se ratio, the ripening started from the lateral surface of the nanosheets and some saw-like nanosheet intermediates were formed. A low acetate/oleate ratio, a low Cd/Se ratio, and a low monomer concentration were found to accelerate the intraparticle ripening of the 2D NCs to form 0D NCs. These findings are useful for the control over the NC shape and size. For example, if we want to design CdSe nanosheets with a large lateral size, we can choose a high Cd/Se ratio, a high precursor concentration, and a medium acetate/oleate ratio (a too high acetate/oleate ratio leads to the formation of nanotubes or aggregated nanosheets). We believe that our work will significantly contribute to the development of controlled synthesis of 2D NCs and quantum dots.

### Limitations of the study

The explanation of porous nanosheet intermediates during the ripening of the nanosheets was related to the growth of nanosheets by particle attachment. However, more solid evidence by electron microscopic technologies to in-situ observe the formation and ripening of the nanosheets are still needed in the future. In addition, the local ligand passivation densities of the internal pores of the porous nanosheet intermediates and the lateral surface of the saw-like intermediates are at present unable to be detected by any techniques, which is important to confirm the ripening mechanism proposed in this work.

## STAR★METHODS

Detailed methods are provided in the online version of this paper and include the following:

- KEY RESOURCES TABLE
- RESOURCE AVAILABILITY
  - Lead contact
  - Materials availability
  - Data and code availability
- METHOD DETAILS
  - Synthesis of CdSe nanotubes
  - Synthesis of CdSe NCs in the presence of both short-chain and medium-/long-chain carboxylate ligands
  - Synthesis of CdSe nanosheets in the presence of butyrate ligand
  - Characterization

## SUPPLEMENTAL INFORMATION

Supplemental information can be found online at https://doi.org/10.1016/j.isci.2021.103457.

## ACKNOWLEDGMENTS

This work was financially supported by Swiss National Science Foundation (No. 200021-146237 and No. P2ELP2_191709) and China Scholarship Council (No.201406360047). The Center Interdépartemental de Microscopie Electronique (CIME) at EPFL is acknowledged for providing the access to SEM and TEM facilities.

## AUTHOR CONTRIBUTIONS

M. G. and V. P. supervised the study. X.H conceived the idea, performed the investigation and characterizations. X.H, M. G., and V. P. analyzed the results. X.H and M. G. wrote and edited the manuscripts.

## DECLARATION OF INTERESTS

The authors declare no competing interests.

Received: October 1, 2021
Revised: November 2, 2021
Accepted: November 10, 2021
Published: December 17, 2021

## REFERENCES

Anderson, N.C., Hendricks, M.P., Choi, J.J., and Owen, J.S. (2013). Ligand exchange and the stoichiometry of metal chalcogenide nanocrystals: spectroscopic observation of facile metal-carboxylate displacement and binding. J. Am. Chem. Soc. *135*, 18536–18548.

Berends, A.C., and de Mello Donega, C. (2017). Ultrathin one-and two-dimensional colloidal semiconductor nanocrystals: pushing quantum confinement to the limit. J. Phys. Chem. Lett. *8*, 4077–4090.

Bertrand, G.H., Polovitsyn, A., Christodoulou, S., Khan, A.H., and Moreels, I. (2016). Shape control of zincblende CdSe nanoplatelets. Chem. Commun. *52*, 11975–11978.

Bouet, C., Tessier, M.D., Ithurria, S., Mahler, B., Nadal, B., and Dubertret, B. (2013). Flat colloidal semiconductor nanoplatelets. Chem. Mater. *25*, 1262–1271.

Chen, Z., Nadal, B., Mahler, B., Aubin, H., and Dubertret, B. (2014). Quasi-2D colloidal semiconductor nanoplatelets for narrow electroluminescence. Adv. Funct. Mater. *24*, 295–302.

Cho, W., Kim, S., Coropceanu, I., Srivastava, V., Diroll, B.T., Hazarika, A., Fedin, I., Galli, G., Schaller, R.D., and Talapin, D.V. (2018). Direct synthesis of six-monolayer (1.9 nm) thick zinc-blende CdSe nanoplatelets emitting at 585 nm. Chem. Mater. *30*, 6957–6960.

Christodoulou, S., Climente, J.I., Planelles, J., Brescia, R., Prato, M., Martín-García, B., Khan, A.H., and Moreels, I. (2018). Chloride-induced thickness control in CdSe nanoplatelets. Nano Lett. *18*, 6248–6254.

Cunningham, P.D., Coropceanu, I., Mulloy, K., Cho, W., and Talapin, D.V. (2020). Quantized reaction pathways for solution synthesis of colloidal ZnSe nanostructures: a connection between clusters, nanowires, and two-dimensional nanoplatelets. ACS Nano *14*, 3847–3857.

Huang, X., Parashar, V., and Gijs, M. (2018). Nucleation and growth behavior of CdSe nanocrystals synthesized in the presence of oleylamine coordinating ligand. Langmuir *34*, 6070–6076.

Huang, X., Parashar, V.K., and Gijs, M.A. (2019). Spontaneous formation of CdSe photoluminescent nanotubes with visible-light photocatalytic performance. ACS Cent. Sci. *5*, 1017–1023.

Huang, X., Parashar, V.K., Ao, Z., and Gijs, M.A. (2020). Insight into the growth of anisotropic CdSe nanocrystals: attachment of intrinsically different building blocks. J. Phys. Chem. C *124*, 27754–27762.

Ithurria, S., and Dubertret, B. (2008). Quasi 2D colloidal CdSe platelets with thicknesses controlled at the atomic level. J. Am. Chem. Soc. *130*, 16504–16505.

Ithurria, S., Bousquet, G., and Dubertret, B. (2011a). Continuous transition from 3D to 1D confinement observed during the formation of CdSe nanoplatelets. J. Am. Chem. Soc. *133*, 3070–3077.

Ithurria, S., Tessier, M., Mahler, B., Lobo, R., Dubertret, B., and Efros, A.L. (2011b). Colloidal nanoplatelets with two-dimensional electronic structure. Nat. Mater. *10*, 936–941.

Ivanov, V.K., Fedorov, P.P., Baranchikov, A.Y., and Osiko, V.V.E. (2014). Oriented attachment of particles: 100 years of investigations of non-classical crystal growth. Russ. Chem. Rev. *83*, 1204.

Kim, W., Lim, S.J., Jung, S., and Shin, S.K. (2010). Binary amine– phosphine passivation of surface traps on CdSe nanocrystals. J. Phys. Chem. C *114*, 1539–1546.

LaMer, V.K., and Dinegar, R.H. (1950). Theory, production and mechanism of formation of monodispersed hydrosols. J. Am. Chem. Soc. *72*, 4847–4854.

Lee, S.M., Cho, S.N., and Cheon, J. (2003). Anisotropic shape control of colloidal inorganic nanocrystals. Adv. Mater. *15*, 441–444.

Li, Z., and Peng, X. (2011). Size/shape-controlled synthesis of colloidal CdSe quantum disks: ligand and temperature effects. J. Am. Chem. Soc. *133*, 6578–6586.

Mahler, B., Nadal, B., Bouet, C., Patriarche, G., and Dubertret, B. (2012). Core/shell colloidal semiconductor nanoplatelets. J. Am. Chem. Soc. *134*, 18591–18598.

Owen, J. (2015). The coordination chemistry of nanocrystal surfaces. Science *347*, 615–616.

Peng, Z.A., and Peng, X. (2001). Mechanisms of the shape evolution of CdSe nanocrystals. J. Am. Chem. Soc. *123*, 1389–1395.

Peng, X., Manna, L., Yang, W., Wickham, J., Scher, E., Kadavanich, A., and Alivisatos, A.P. (2000). Shape control of CdSe nanocrystals. Nature *404*, 59–61.

Riedinger, A., Ott, F.D., Mule, A., Mazzotti, S., Knüsel, P.N., Kress, S.J., Prins, F., Erwin, S.C., and Norris, D.J. (2017). An intrinsic growth instability in isotropic materials leads to quasi-two-dimensional nanoplatelets. Nat. Mater. *16*, 743–748.

Rossinelli, A.A., Riedinger, A., Marqués-Gallego, P., Knüsel, P.N., Antolinez, F.V., and Norris, D.J. (2017). High-temperature growth of thick-shell CdSe/CdS core/shell nanoplatelets. Chem. Commun. *53*, 9938–9941.

Schliehe, C., Juarez, B.H., Pelletier, M., Jander, S., Greshnykh, D., Nagel, M., Meyer, A., Foerster, S., Kornowski, A., and Klinke, C. (2010). Ultrathin PbS sheets by two-dimensional oriented attachment. Science *329*, 550–553.

She, C., Fedin, I., Dolzhnikov, D.S., Demortière, A., Schaller, R.D., Pelton, M., and Talapin, D.V. (2014). Low-threshold stimulated emission using colloidal quantum wells. Nano Lett. *14*, 2772–2777.

She, C., Fedin, I., Dolzhnikov, D.S., Dahlberg, P.D., Engel, G.S., Schaller, R.D., and Talapin, D.V. (2015). Red, yellow, green, and blue amplified spontaneous emission and lasing using colloidal CdSe nanoplatelets. ACS Nano *9*, 9475–9485.

Son, J.S., Yu, J.H., Kwon, S.G., Lee, J., Joo, J., and Hyeon, T. (2011). Colloidal synthesis of ultrathin two-dimensional semiconductor nanocrystals. Adv. Mater. *23*, 3214–3219.

Uematsu, T., Baba, M., Oshima, Y., Tsuda, T., Torimoto, T., and Kuwabata, S. (2014). Atomic resolution imaging of gold nanoparticle generation and growth in ionic liquids. J. Am. Chem. Soc. *136*, 13789–13797.

Vondrásek, J.Í., Mason, P.E., Heyda, J., Collins, K.D., and Jungwirth, P. (2009). The molecular origin of like-charge arginine– arginine pairing in water. J. Phys. Chem. B *113*, 9041–9045.

Wang, F., Wang, Y., Liu, Y.-H., Morrison, P.J., Loomis, R.A., and Buhro, W.E. (2015). Two-dimensional semiconductor nanocrystals: properties, templated formation, and magic-size nanocluster intermediates. Acc. Chem. Res. *48*, 13–21.

Whitehead, C.B., Özkar, S., and Finke, R.G. (2019). LaMer's 1950 model for particle formation of instantaneous nucleation and diffusion-controlled growth: a historical look at the model's origins, assumptions, equations, and underlying sulfur sol formation kinetics data. Chem. Mater. *31*, 7116–7132.

You, H., and Fang, J. (2016). Particle-mediated nucleation and growth of solution-synthesized metal nanocrystals: a new story beyond the LaMer curve. Nano Today *11*, 145–167.

Yu, J., and Chen, R. (2020). Optical properties and applications of two-dimensional CdSe nanoplatelets. Info. Mat. *2*, 905–927.

Yu, W.W., Qu, L., Guo, W., and Peng, X. (2003). Experimental determination of the extinction coefficient of CdTe, CdSe, and CdS nanocrystals. Chem. Mater. *15*, 2854–2860.

## STAR★METHODS

### KEY RESOURCES TABLE

| REAGENT or RESOURCE | SOURCE | IDENTIFIER |
|---|---|---|
| Chemicals, peptides, and recombinant proteins | | |
| Cadmium oxide | Sigma-Aldrich | CAS:1306-19-0 |
| Cadmium acetate hydrate | Sigma-Aldrich | CAS:89,759-80-8 |
| 1-Octadecene | Sigma-Aldrich | CAS:112-88-9 |
| Hexanoic acid | Sigma-Aldrich | CAS:142-62-1 |
| Octanoic acid | Sigma-Aldrich | CAS:124-07-2 |
| Lauric acid | Sigma-Aldrich | CAS:143-07-7 |
| Oleic acid | Sigma-Aldrich | CAS:112-80-1 |
| Dioctylamine | Sigma-Aldrich | CAS:1120-48-5 |
| Trioctyl phosphine | Sigma-Aldrich | CAS:4731-53-7 |
| Selenium powder | Sigma-Aldrich | CAS:7782-49-2 |
| Methanol | Sigma-Aldrich | CAS:67-56-1 |
| Hexane | Sigma-Aldrich | CAS:110-54-3 |
| Ethanol | Sigma-Aldrich | CAS:64-17-5 |
| Dichloromethane | Sigma-Aldrich | CAS:75-09-2 |
| Butyric acid | Fluka | CAS:107-92-6 |
| Other | | |
| UV-vis spectrophotometer | Varian Cary 50, Agilent | https://www.agilent.com/en/product/molecular-spectroscopy/uv-vis-uv-vis-nir-spectroscopy |
| Fluorescence spectrometer | Horiba | https://www.horiba.com/ind/products/by-segment/scientific/molecular-and-microanalysis/fluorescence-spectroscopy/ |
| Transmission electron microscope | Talos F200S, FEI | https://www.fei.com/talos-f200i/#gsc.tab=0 |
| Fouriertransform infrared spectroscope | Nicolet iS10, Thermo Fisher Scientific | https://www.thermofisher.com/order/catalog/product/IQLAADGAAGFAHDMAPC |
| Thermal gravimetric analysis (TGA) | TGA 4000, Perkin Elmer. | https://www.perkinelmer.com.cn/product/tga-4000-system-100-240v-50-60hz-n5370210 |
| Powder X-ray diffractometer | Empyrean, Malvern Panalytical | https://www.malvernpanalytical.com/en/products/product-range/empyrean-range/empyrean |

### RESOURCE AVAILABILITY

#### Lead contact

Further information and requests for resources and reagents should be directed to and will be fulfilled by the lead contact, Martin Gijs (martin.gijs@epfl.ch).

#### Materials availability

This study did not generate new unique reagents. All chemicals were obtained from commercial resources and used as received.

#### Data and code availability

- All data reported in this paper will be shared by the lead contact upon request.
- No new code was generated during the course of this study.
- Any additional information required to reanalyze the data reported in this paper is available from the lead contact upon request.

## METHOD DETAILS

### Synthesis of CdSe nanotubes

Synthesis of the CdSe nanotubes is based on the modification of a previously reported method (Huang et al., 2019). A stock solution label as "$Cd(Ac)_2$-DOAm solution" was first prepared as follows. 333 mg (1.25 mmol) of $Cd(Ac)_2 \cdot 2H_2O$ were sonicated in 1.5 mL (5 mmol) of DOAm (a molar ratio of 1:4 between Cd and DOAm was taken), followed by heating at 200°C for 10 min to fully remove the water and get a clear solution. A stock TOP-Se solution (1.5 MLs) was prepared by injecting 6.67mL of trioctylphosphine (TOP) into the 790 mg (10 mmol) of selenium powder under the protection of argon atmosphere. It was kept stirring for more than 12 h to ensure complete dissolution and finally stored in a sealed flask. In a typical protocol of CdSe nanotubes synthesis, 0.1 mmol of TOP-Se solution was first mixed with 2 mL of ODE and stirred at 260°C for 5 min. Then, 0.25 mmol of $Cd(Ac)_2$-DOAm solution (a molar ratio of 2.5:1 between Cd and Se) was quickly injected. The solution rapidly turned turbid, followed by a change in color from white into yellow, and finally into a brown solution. After a given time (e. g. 8 min), the reaction was stopped by removal of the heater and the mixture was cooled down to room temperature. The ripened nanostructures were obtained after a longer reaction time (e. g. 256 min). To purify the sample, the cooled solution was first mixed with 0.2 mL of oleic acid at room temperature, then washed by a dispersion and centrifugation process in a hexane-ethanol solution (1:1, v/v) twice and in a methanol solution twice. The methanol is used to remove the unreacted Cd precursor. Finally, the precipitates were dispersed in hexane for further characterization.

### Synthesis of CdSe NCs in the presence of both short-chain and medium-/long-chain carboxylate ligands

Most of the CdSe NCs in this work are prepared in the presence of cadmium acetate and a medium-chain or a long-chain carboxylate ligand based on the protocol of CdSe nanotubes synthesis. Taking the sample in Figure 2 of the text as an example, 0.5 mmol of oleic acid and 0.1 mmol of TOP-Se solution was mixed with 2 mL of ODE and stirred at 260°C for 10 min. After that, 0.25 mmol of $Cd(Ac)_2$-DOAm solution (a molar ratio of 1:1 between acetate and oleate) was quickly injected. A small amount of the solution (~200 μL) was fetched at different time intervals for further analysis. To purify the sample, the cooled solution was washed by a dispersion and centrifugation process in a dichloromethane-methanol solution (2:1, v/v) twice. The final precipitates were dispersed in hexane for further characterization. In Figures 1B–1D of the text, the oleic acid was replaced by other carboxylic acids including hexanoic acid, octanoic acid and lauric acid to form hexanoate, octanoate or laurate ligands on the surface of the NCs. In Figure S4 of the supplemental information, the amount of oleic acid was changed while the amounts of $Cd(Ac)_2$-DOAm solution and TOP-Se solution were fixed at 0.25 mmol and 0.1 mmol. In Figures 3 of the text and S5 of the supplemental information, the amounts of $Cd(Ac)_2$-DOAm solution and TOP-Se solution were changed while the molar ratio between the acetate and oleate was fixed at 1:0.25.

### Synthesis of CdSe nanosheets in the presence of butyrate ligand

The multi-layered CdSe nanosheets passivated by the butyrate ligand were prepared with minor modification of a reported method (Huang et al., 2020). Typically, 128 mg (1 mmol) of CdO powders was mixed with 2 mmol of butyric acid in a 5 mL vial, vigorously vibrated for 5 min and then heated at 200°C, resulting in a clear cadmium butyrate solution. Afterward, 1.2 mL (4 mmol) of DOAm solution was added and the mixture was heated for 5 min to get a clear solution, which was labeled as "$Cd(butyrate)_2$-DOAm solution". To synthesize the CdSe nanosheets, 0.1 mmol of TOP-Se solution (1.5 M) was added into 2 mL of ODE and stirred at 260°C for 5 min, after which 0.25 mmol of $Cd(butyrate)_2$-DOAm solution was quickly injected. The reaction was kept at 260°C for a given time. A small amount of the solution (~200 μL) was fetched at different time intervals for further analysis. To purify the sample, the cooled solution was washed by a dispersion and centrifugation process in a hexane-ethanol solution (1:1, v/v) twice and in a methanol solution twice. Finally, the precipitates were dispersed in hexane for further characterization.

### Characterization

UV-vis absorption spectroscopy was performed on a Varian Cary 50 Scan UV-vis spectrophotometer. Photoluminescence (PL) spectra were measured by Horiba fluorescence spectrometer, in which the excitation wavelength was set as 350 nm. Transmission electron microscopy (TEM) graphs, scanning transmission electron microscopy (STEM) images were captured by a Talos transmission electron microscope (FEI Co.); prior to that, the CdSe NCs dissolved in hexane were dropped and dried on ultrathin carbon-supported

copper grids. Fouriertransform infrared spectroscopy (FTIR) spectra were recorded by a Nicolet iS10 FT-IR Spectrometer (Thermo Scientific) equipped with a smart diamond attenuated total reflectance (ATR) accessory. Thermal gravimetric analysis (TGA) curve was measured by a TGA 4000 from PerkinElmer. The TGA data were obtained by heating the samples from 30°C to 600°C in the air atmosphere at a speed of 10°C/min. Powder X-ray diffraction (PXRD) measurement was performed on Empyrean with Cu LEF sealed tube and Pixcel1D detector from PANalytical.